Energy Conversion and Management 119 (2016) 37–48

Contents lists available at ScienceDirect

Energy Conversion and Management

journal homepage: www.elsevier.com/locate/enconman

Parameter estimation of photovoltaic modules using iterative method and the Lambert W function: A comparative study

I. Nassar-eddine, A. Obbadi *, Y. Errami, A. El fajri, M. Agunaou

Laboratory: Electronics, Instrumentation and Energy (LEIE), Team: Exploitation and Processing of Renewable Energy (EPRE), Faculty of Science, Chouaib Doukkali University, Department of Physics, Route Ben Maachou, 24000 El Jadida, Morocco

ARTICLE INFO

Article history:
Received 8 January 2016
Received in revised form 12 March 2016
Accepted 9 April 2016

Keywords:
Various photovoltaic (PV) module
Single diode model
Estimation methods
Mathematical models
Lambert W function
RMSE

ABSTRACT

This paper presents a comparative study of the parameter estimation methods which are based exclusively on the manufacturer's datasheets, for various technologies of photovoltaic (PV) modules, using the single diode five parameter model. Accurate determination of these parameters which arose from a diversification of models and methods dedicated to their estimations is still a challenge for researchers. In this study, two parameter estimation methods are employed: an iterative method which adjusts the series resistance and an analytical method based on the Lambert W function. These methods are used to calculate the five unknown parameters at Standard Test Conditions (STC) of three types of PV modules using different technologies, namely multicrystalline, monocrystalline, and thin-film. Five existing mathematical models are implemented to estimate the parameters of these PV modules under changing environmental conditions. These five models are classified from 1–5 for both parameter estimation methods. Each model is based on the combination of the reverse saturation current and the photocurrent. Then, the results of the different models simulations are compared with the measured data, which are extracted from datasheet characteristics in order to validate the reliability and evaluate the accuracy of the five models. The results of the implanted models indicate a high agreement between the measured data and the simulated *I–V* characteristics under varying temperature and irradiance. Moreover, the use of the Root Mean Square Error (RMSE) presents a good accuracy indicator for both methods. On the one hand, the results show that the combination of the analytical method of estimation with all five models guarantees the fewest errors between the estimated and measured data for the thin-film module under varying environmental conditions, especially at low temperature and high irradiance. On the other hand, the behavior of the two methods is almost the same for the monocrystalline and multicrystalline modules.

Contents

* Corresponding author.
E-mail addresses: ilham.nassareddine20@gmail.com (I. Nassar-eddine), obbadi.a@ucd.ac.ma (A. Obbadi), errami.y@ucd.ac.ma (Y. Errami), elfajri@hotmail.com (A. El fajri), mostaf_agn@yahoo.fr (M. Agunaou).

http://dx.doi.org/10.1016/j.enconman.2016.04.030
0196-8904/

Nomenclature

STC	Standard Test Conditions
I	the output current (A)
I_d	diode current (A)
I_{Rp}	parallel resistance current (A)
I_{PV}	photocurrent generated by the module (A)
I_{pvn}	photocurrent at STC (A)
I_S	diode reverse saturation current (A)
I_{Sn}	diode reverse saturation current at STC (A)
R_S	series resistance (Ω)
R_P	parallel resistance (Ω)
$R_{p,\min}$	minimum value of parallel resistance (Ω)
R_{P0}	value of R_P (Ω) at short circuit point (0, I_{SC})
A	diode ideality factor
N_S	number of cells in series
V	the output voltage (V)
V_t	thermal voltage (V)
V_{tn}	thermal voltage at STC (V)
K	Boltzmann's constant (=1.3806 × 10^{-23} J/K)
q	electron charge (=1.602 × 10^{-19} C)
T	temperature of the module (K)
T_n	temperature of the module at STC (=298 K)
G	irradiance of the module (W/m^2)
G_n	irradiance of the module at STC (W/m^2)
I_{sc}	short circuit current (A)
I_{scn}	short circuit current at STC (A)
V_{oc}	open circuit voltage (V)
V_{ocn}	open circuit voltage at STC (V)
V_{mpp}	maximum power voltage (V)
I_{mpp}	maximum power current (A)
$P_{\max,m}$	calculated value of maximum power (W)
$P_{\max,e}$	experimental value of maximum power (W)
K_I	current temperature coefficient (A/°C)
K_V	voltage temperature coefficient (V/°C)
E_g	band gap energy (eV)
dT	the temperature difference ($dT = T - T_n$) (K)

1. Introduction

Photovoltaic (PV) energy is currently experiencing strong growth worldwide. In Morocco, this development is boosted by a national policy that aims to reduce gas emissions by 13% by 2030 [1,2]. This reduction could reach 32% with enough international financial support [1,2]. Looking ahead, Morocco's national energy strategy is aiming to raise the share of renewable energy to 42% of the total installed capacity in the country by 2020, with solar, wind and hydro each contributing 14%. The country's ambitions grow in 2015 and Morocco is now determined to achieve a 52% share of renewables electricity generation capacity by 2030 according to the Moroccan announcement at COP21 (Conference of Parties) [1]. PV energy has become a way of producing electricity in addition to hydro and wind power In 2012, Morocco had a total capacity of 14 MWc divided between stand-alone PV systems (approximately 12 MWc) and grid-connected PV sites (approximately 2 MWc) installed as part of several programs such as PERG (Global Rural Electrification Program) and CHOUROUK program during the 2000s [2]. To increase the security of electricity supply and the quality of service in isolated regions, several sites have recently been identified for the large-scale collection of solar power. The largest of these sites to be developed is Noor solar complex which will be the world's largest solar site with a total power of 580 MW [2]. The first part of the complex is the Noor I Concentrated Solar Power (CSP) plant in Ouarzazate with a total power of 160 MW [2]. In July 2015, Morocco implemented a program to build several PV plants, namely the Noor-Tafilalt, Noor-Atlas, and Noor-Argana projects with a total power of 400 MWc connected to the high voltage network (HV: 60 kV) [2]. The Moroccan electricity and water utility company ONEE has decided to raise the capacity of the forthcoming Noor-Argana photovoltaic tender to 200 MW from 125 MW, bringing the total capacity of its photovoltaic program to 500 MW by 2018 [2]. From a legal point of view and in its endeavor to face energy and environmental issues, Morocco decided in 2009 to give impetus to the development of renewable energies by enacting several laws [1,3]. The last one of them is the law 58–15 which modifies and complements the existing 13–09 law on renewable energy to introduce a net metering scheme for solar and wind power plants connected to the high-voltage grid, and later, those connected at the middle and low-voltage level as well [1]. Private investors in renewable power will be able to sell their surplus output to the grid, but no more than 20% of their annual production [1]. Investors in PV will also benefit from the opening of the low-voltage grid to renewable power installations. Another use of solar energy is Solar Water Heating (SWH), for which the technical feasibility in residential buildings was assessed by Allouhi et al. [4] under Moroccan climatic conditions. In order to perform annual simulations of the SWH system, six climatic zones were used according to the recent climatic zoning established by ADEREE (National Agency for the Development of Renewable Energy and Energy Efficiency). They found that most Moroccan cities have significant potential in implementing SWH systems, and that the use of Evacuated Tube Collectors (ETC) is preferable and more suitable than Flat Plat Collectors (FPC) from a technical point of view. Furthermore, solar energy is also present in another application where biomass energy is converted into solar fuel in solar pyrolysis process. In this context, Zeng et al. [5] used a Box–Behnken experimental design/design of experiments to optimize solar pyrolysis process to produce combustible gases from beech wood, and found that wood energy content is upgraded by solar pyrolysis. Energy efficiency is generally based on the optimization of energy consumption and emissions of greenhouse gases. In this context, several solutions have appeared such as smart grids and nZEB (nearly-Zero Energy Buildings). Najibi and Niknam [6] introduced a new model of PV array by simulating and testing it on one typical Micro-Grid to see its performance regarding optimal energy management of Micro-grids,

while, Cao and Sirén [7] implemented nZEB methodology in the twofold problem of on-site matching and hybrid–grid interactions. In both works, the results show that the developed methodology can seek an optimized balance between the objectives of maximizing the matching capability and minimizing the environmental/economic load. Therefore, PV solar panels are included as an ideal solution for generating electricity at home. Investments in the residential sector offer greater profitability per unit of installed power capacity than in commercial and industrial sectors. Indeed, self-consumption is an effective way to monetize the PV panels. In this context, Chiaroni et al. [8] analyze the profitability of investment in the realization of photovoltaic facilities in a mature market such as Italy with a focus on the role of self-consumption. This market is characterized by the absence of support mechanisms for PV sources for electricity and by a high level of maturity in the energy market. Other recent studies have examined the economic impact of solar PV in other countries. For example, De Arce et al. [9] identify different future deployment of renewable sources of energy, including solar PV, in an emerging market like Morocco, and simulate their economic effects over the next 30 years. The overall figures for the economic impact on gross domestic product is found to be 1.21–1.99% by 2040 and the employment effect is 269,252–499,000 jobs.

The most frequent barrier which arises in almost every country and which may slow down the introduction of renewable energy is that of public acceptance and permission. Hanger at al. [10] investigate the issue of community acceptance of CSP installations in the Moroccan context and conclude that community acceptance is almost universal, particularly because solar power is perceived to be environmentally friendly, has a socio-economic contribution to the cultural development of the region, and offers access to several nearby villages as well as an emergence of new tourism products. The development of renewable energy usage depends on several factors such as political strategic decisions and geographical situation [11]. Indeed the high development of renewable energy requires overcoming supply chain. In this context, Cucchiella and D'Adamo [11] indicate the importance of implementing a supply chain that is sustainable environmentally, economically and socially. This importance is illustrated by an improvement in the profitability of our company and in our protection of the environment.

All factors considered, the major objective of the researchers and the industry is to improve the power quality of PV systems [12]. Improving the quality of the energy supplied by the PV modules is strongly dependent on their modeling, which is mainly to express mathematically the behavior of a PV module's current and power with respect to the voltage under varying temperature and irradiance [13]. That is why it is very important to design a specific and comprehensive mathematical model of a photovoltaic module. According to the literature, the single diode model and the double diode model [14,15] have frequently been used. In the case reported by this paper, a single diode five parameter model will be used since it offers a good compromise between simplicity and accuracy [13]. The accuracy of a PV module depends on the accuracy of PV mathematical models and on methods for estimating PV module's parameters. Estimation methods are essential in the calculation of the parameters during the design and simulation of PV models. For this reason, various proposed approaches are reviewed in the next section to estimate the unknown parameters of a PV module. Most of them show that the modeling of a photovoltaic system was conducted at Standard Test Conditions (STC) as well as under varying environmental conditions to see the effect of temperature and irradiance on the five parameters: the ideality factor A, the series resistance R_S, the parallel resistance R_P, the photocurrent I_{PV}, and the reverse saturation current I_S. Other approaches used translation equations to estimate the I–V characteristic at any temperature and irradiance based on the known I–V characteristic and PV module parameters at STC. On the one hand, some of the latter approaches have assumed that the R_S, R_P, and A are independent of irradiance and temperature, and that the only parameters which vary with temperature and irradiance are I_{PV} and I_S [16]. On the other hand, authors like Chin and Bai [14,17] have taken into consideration the variation of R_s, R_p and A according to different environmental conditions. This paper focuses on models which consider constant the parameters R_S, R_P and A under varying environmental conditions, which is the most common practice in the literature. In light of this, two estimation methods, an iterative method which adjusts the series resistance [18] and an analytical method based on the Lambert W function [19], are evaluated in order to calculate the five unknown parameters at STC. For both estimation methods, five existing models, which translate the values of the parameters to any irradiance and temperature operating condition, are implemented. Therefore using five combinations expressing the parameters I_{PV} and I_S as functions of temperature and irradiance are obtained and classified into models 1 to 5: Model 1 [13–15], model 2 [13–15], model 3 [13–15,20,21], model 4 [13–15] and model 5 [22].

The main objective of this study is to compare the two aforementioned estimation parameter methods and evaluate their effect on the I–V characteristics models. The present work provides a comparative analysis of the five models classified above in order to choose which method/model combination is better for each PV module technology. This comparison is based on two steps. The first one is to calculate the five parameters at STC for two different parameter estimation methods, the iterative Newton–Raphson method [18], and the analytical method using the Lambert W function [19]. The second one is to validate and verify the accuracy of the five translation models. To achieve that, the I–V characteristics are plotted for three selected PV modules while varying temperature and irradiance. The selected PV modules cover three different PV module technologies: Multicrystalline (Kyocera KC2000GT) [23], Monocrystalline (Shell SQ80) [24], and Thin-film (Shell ST40) [24]. A comparison of their I–V characteristics with the points measured was made for both methods and the results showed good agreement. As a statistical analysis indicator the RMSE of the voltage and current was used in order to assess the accuracy of the different modeling methods, and eventually validate the estimated parameters. Another contribution of the study is envisaged to be as a reference for both new and experienced researchers in the field of PV modeling and simulation. Furthermore, the results from each model were first verified for correctness against the results produced by their respective authors. The simulation of all methods and mathematical models is developed in a MATLAB/Simulink environment.

The rest of this paper is organized as follows: In Section 2 a literature review on parameter estimation methods is given. Section 3 describes the two parameter estimation methods used and briefly presents all the five models with their equivalent equations. Section 4 shows the results obtained from the simulations, which demonstrate the dependence of the five models upon varying environmental conditions, and in order to validate these results, the use of the RMSE is required. The conclusion is given in Section 5.

2. Literature review on parameter estimation methods

According to the literature, several methods have been developed to calculate the five parameter models using the basic information provided in the manufacturer's datasheet. It is found that in general these methods can be classified into three categories namely analytic, iterative, and evolutionary methods [25]. However, these methods have shown different levels of accuracy [26].

Analytical methods are widely used to estimate PV module parameters. They solve only explicit mathematical equations, are very simple, and need far less computational time as only a single iteration is required [25]. These methods perform efficiently at STC for some models as well as under changing environmental conditions. Some of these methods were proposed using the Lambert W function to estimate the parameters of the PV module. For example, Femia et al. [19] proposed a method to calculate analytically the resistances R_S and R_P using Lambert W function. This method expresses the output current of the PV module as an explicit function of its voltage and presents good performance in convergence. Similarly, Batzelis et al. [27] presented another characteristic which expresses voltage with respect to current by using the Lambert W function. Hence, this method combines the versatility and accuracy provided by the single diode model with a significantly faster and more robust execution. Cubas et al. [28] presented a method based on analytical formulation which transformed the series resistance equation into an explicit one by using the Lambert W function. The latter method was used to analyze a commercial PV module's performance at different levels of irradiance and temperature. In addition, Khatib et al. [29] proposed a simple PV module's mathematical model based on the relations between PV module parameters and meteorological variables such as irradiance and ambient temperature. Furthermore, Bai et al. [17] proposed a new compound method: a piecewise fitting method combined with the four parameter model to simplify the calculation procedures for obtaining the five parameters.

The best estimation approach is to formulate a system of equations from the manufacturer datasheets [21,22]. It is difficult to solve this system of transcendental equations analytically, but it can be solved by numerical methods [26]. A number of iterative methods are available in the literature. Among these iterative methods are probably the best options for parameter estimations. The Newton Raphson method (NRM) is one of the best root-finding methods [13,14,18], but improper choice of the initial conditions affects its accuracy and convergence. Villalva and Moballegh [18,30] chose values of series resistance starting from zero and building up the resistance until a specified and acceptable margin of error exists between the calculated value and the maximum power point values. Siddique and Rahman [22,31] used the same idea, but instead of adjusting the resistance R_S, they varied the ideality factor between 1 and 2. Mahmoud et al. [21] proposed another method to evaluate the parallel resistance R_P where the other four parameters are calculated from a system of equations. Meanwhile, Navabi et al. [32] used a simple iterative process to determine the overall PV plant parameters for any time and operating condition. Mares et al. [33] improved and implemented a modified procedure for solving the five parameters non-linear system of equations which is a modified version of the bisection method that guarantees the convergence of the numerical algorithm.

Recently, evolutionary methods which use artificial intelligence techniques have been extensively used in PV parameter estimation due to their accuracy and reliability in terms of performance. Much work has been carried out using some of the popular evolutionary algorithms like Genetic Algorithms (GA) [20], Particle Swarm Optimization (PSO) [34], Simplified Bird Mating Optimizer (SBMO) [35], Cat Swarm Optimization (CSO) [36], Artificial Bee Swarm Optimization (ABSO) [37], Bacterial Foraging (BF) [38], Flower Pollination Algorithm (FPA) [39], Differential Evolution with Adaptive Mutation (DEAM) [40], Evolutionary Algorithm (EA) based on analytical method [41], and Artificial Neural Network (ANN) [42,43]. Ismail et al. [20] utilized the optimization ability of a genetic algorithm in order to obtain the parameters of a PV model under varying temperatures and irradiances as well as partial shading conditions. Alam et al. [39] proposed a new optimization method FPA, which has the highest speed of conversion to the optimal solution with the shortest convergence time, in order to estimate the optimal parameters of single and double diode models. This method is simple, very efficient and can outperform both GA and PSO. Muhsen et al. [40] proposed using DEAM, which utilizes attraction–repulsion to boost the mutation operation of the original DE, a method which offers high accuracy, rapid convergence, and optimal adjusted control parameters. Barukčić et al. [41] used an analytical function to express the dependencies of the parameters on temperature and irradiance, which are then estimated using an evolutionary algorithm. Fathabadi et al. [43] proposed a novel neural-analytical technique, which is based on the application of feed-forward artificial neural network together with Lambert W function.

Some researchers have compared the estimation methods of PV models with the aim of determining which method surpasses the others in terms of accuracy, efficiency and convergence. For example, Tamrakar and Gupta [25] presented a survey on parameter estimation of PV module model and its recent advances. They concluded that analytical methods required less computational time but some of them were still unable to find all the parameters, that iterative methods suffered from convergence problems, and that evolutionary methods were best for fast varying weather conditions and partial shading conditions, although they might suffer from premature convergence in the case of improper selection of control parameters and initial conditions. Chin et al. [14] deliberated and reviewed important works on the modeling and parameter estimation methods of PV module. Humada et al. [15] discussed, summarized and classified the techniques for parameter estimation as well as the reviewed models on the basis of the number of estimated parameters.

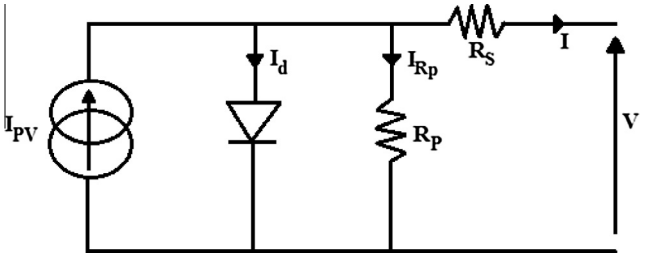

Fig. 1. Equivalent circuit of single diode five parameter model.

3. The equivalent model of a photovoltaic module

The main goal of modeling is to represent the nonlinear behavior of a photovoltaic module by an equivalent electrical circuit, which is shown at Fig. 1. Modeling requires two steps. The first is the estimation of the unknown parameters and the second is the use of these parameters in the simulation of different mathematical models to study the influence of environmental change on the behavior of these modules [13].

The characteristic equation of the single diode five parameter model is given by [13,14]:

$$I = I_{PV} - I_S \cdot \left[\exp\left(\frac{V + R_S \cdot I}{A \cdot N_S \cdot V_t}\right) - 1\right] - \frac{V + R_S \cdot I}{R_P} \quad (1)$$

where

$$V_t = \frac{k \cdot T}{q} \quad (2)$$

In general, the five parameters I_{PV}, I_S, A, R_S and R_P in Eq. (1) are the unknown parameters to be calculated. To determine their values, a system of independent equations is required and can be

obtained by exploiting the three remarkable points of the *I–V* characteristic at STC. These points are substituted into Eq. (1) resulting in the following equations:At open circuit point (V_{OC}, 0):

$$0 = I_{PV} - I_S\left[\exp\left(\frac{V_{OC}}{A\cdot N_S\cdot V_t}\right)-1\right]-\frac{V_{OC}}{R_P} \tag{3}$$

At short circuit point (0, I_{SC}):

$$I_{SC} = I_{PV} - I_S\left[\exp\left(\frac{R_S\cdot I_{SC}}{A\cdot N_S\cdot V_t}\right)-1\right]-\frac{R_S\cdot I_{SC}}{R_P} \tag{4}$$

And

$$\left.\frac{dI}{dV}\right|_{\substack{V=0\\ I=I_{SC}}} = \frac{-1}{R_{P_0}} \tag{5}$$

At maximum power point MPP (V_{mpp}, I_{mpp}):

$$I_{mpp} = I_{PV} - I_S\left[\exp\left(\frac{V_{mpp}+I_{mpp}\cdot R_S}{A\cdot N_S\cdot V_t}\right)-1\right]-\frac{V_{mpp}+I_{mpp}\cdot R_S}{R_P} \tag{6}$$

And

$$\left.\frac{dP}{dV}\right|_{\substack{V=V_{mpp}\\ I=I_{mpp}}} = 0 \tag{7}$$

It is difficult to solve this system of equations analytically. Thus, the use of numerical methods is essential to calculate the unknown parameters.

3.1. The estimation methods of photovoltaic parameters

The estimation of the unknown parameters at STC is carried out by various methods. In this work, we chose two different methods. The first, designated Method I, uses the iterative method based on the adjustment of R_S [18], which is based on the Newton–Raphson algorithm. The second, designated Method II, uses an analytical method based on the Lambert W function [19] to solve a set of equations.

After obtaining the five parameters at the required condition, these parameters can then be substituted in the *I–V* equation to obtain the currents which are themselves functions of Eq. (1), iterative technique had to be applied. The iterative technique applied in this work is the Newton–Raphson method as given by (8). The corresponding equivalent for Eq. (1) can be written as (9).

$$f(x)_{n+1} = f(x)_n + \frac{df(x)}{dx} \tag{8}$$

$$I_{n+1} = I_n - \frac{I_{pv} - I_n - I_s\left(\exp\left(\frac{V+I_n\cdot R_s}{A\cdot N_s\cdot V_t}\right)-1\right)}{-1-\frac{I_s\cdot R_s}{A\cdot N_s\cdot V_t}\left(\exp\left(\frac{V+I_n\cdot R_s}{A\cdot N_s\cdot V_t}\right)-1\right)} \tag{9}$$

3.1.1. Estimation method I

This method presents an easy and accurate way to reduce the number of equations to four by adjusting the resistance R_S. The resistances R_S and R_P can then be computed from the fact that only a unique pair of these two parameters gives the maximum power at every operating condition. This unique pair can be obtained using the iterative method by gradually adjusting the values of R_S and then calculating the corresponding value of R_P which gives a close approximation to the maximum experimental power obtained from the datasheet. Villalva and Gazoli [18] and Moballegh and Jiang [30] used this method. The expressions of the various parameters are given by the following equations:

Under the short circuit condition, the exponential term tends to 1 as R_S is very low. Therefore, the expression of I_{PV} described in [18] becomes:

$$I_{pvn} = \frac{R_S + R_P}{R_P}\cdot I_{sc} \tag{10}$$

At the initial conditions $R_S = 0$, Eq. (10) reduces to:

$$I_{pvn} = I_{sc} \tag{11}$$

Taking into account that R_P is very high, Eq. (1) becomes:

$$I = I_{pv} - I_S\cdot\left[\exp\left(\frac{V+R_S\cdot I}{A\cdot N_S\cdot V_t}\right)-1\right] \tag{12}$$

And Eq. (3) is given by:

$$0 = I_{pvn} - I_S\left[\exp\left(\frac{V_{OC}}{A\cdot N_S\cdot V_t}\right)-1\right] \approx I_{pvn} - I_S\cdot\exp\left(\frac{V_{OC}}{A\cdot N_S\cdot V_t}\right) \tag{13}$$

In the above equation, the second equivalence was obtained by neglecting the term '1' ahead of the exponential. Therefore, V_{OC} at STC can be expressed as follows:

$$V_{ocn} \approx A\cdot N_S\cdot V_{tn}\cdot\ln\left(\frac{I_{pvn}}{I_{Sn}}\right) \tag{14}$$

The voltage temperature coefficient K_V can be calculated by use of the following expression:

$$K_V = \frac{dV_{ocn}}{dT} = \frac{d}{dT}\left[A\cdot N_S\cdot V_{tn}\cdot\ln(I_{pvn}) - A\cdot N_S\cdot\ln(I_{sn})\right] \tag{15}$$

Hence:

$$K_V = \frac{A\cdot N_S\cdot V_{tn}}{T_n}\cdot\ln\left(\frac{I_{pvn}}{I_{Sn}}\right) + A\cdot N_S\cdot V_{tn}\left[\frac{1}{I_{pvn}}\cdot\frac{dI_{pvn}}{dT} - \frac{1}{I_{Sn}}\cdot\frac{dI_{Sn}}{dT}\right] \tag{16}$$

The term between brackets in the equation above can be calculated by means of the following Eqs. (17) and (18) [19]:

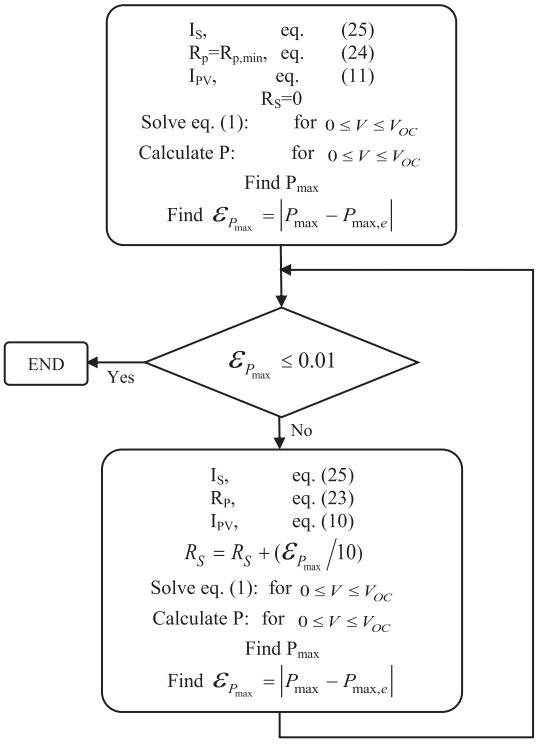

Fig. 2. R_S calculation flow chart [18].

$$K_i = \frac{dI_{pvn}}{dT} \tag{17}$$

$$\frac{1}{I_{Sn}} \cdot \frac{dI_{Sn}}{dT_n} = \frac{3}{T_n} + \frac{E_g}{k \cdot T_n^2} \tag{18}$$

Thus Eq. (16) becomes:

$$K_V = \frac{A \cdot N_S \cdot V_{tn}}{T_n} \cdot \ln\left(\frac{I_{pvn}}{I_{Sn}}\right) + A \cdot N_S \cdot V_{tn}\left[\frac{K_i}{I_{pvn}} - \frac{3}{T_n} - \frac{E_g}{k \cdot T_n^2}\right] \tag{19}$$

Substituting Eq. (14) into Eq. (19) yields:

$$K_V = \frac{V_{OCn}}{T_n} + A \cdot N_S \cdot V_{tn}\left[\frac{K_i}{I_{pvn}} - \frac{3}{T_n} - \frac{E_g}{k \cdot T_n^2}\right] \tag{20}$$

Rearranging Eq. (20), we can express the ideality factor as:

$$A = \frac{K_V - \frac{V_{ocn}}{T_n}}{A \cdot N_S \cdot V_{tn} \cdot \left(\frac{K_i}{I_{pvn}} - \frac{3}{T_n} - \frac{E_g}{k \cdot T_n^2}\right)} \tag{21}$$

At MPP the resistance R_P can be calculated using the Eq. (22).

$$P_{\max,m} = P_{\max,e} = V_{mpp}\left\{I_{pv} - I_S\left[\exp\left(\frac{V_{mpp} + R_S \cdot I_{mpp}}{A \cdot N_S \cdot V_t}\right) - 1\right] - \frac{V_{mpp} + R_S \cdot I_{mpp}}{R_p}\right\} \tag{22}$$

Rearranging Eq. (22) R_P is calculated by means of Eq. (23).

$$R_p = \frac{V_{mpp}(V_{mpp} + I_{mpp} \cdot R_S)}{V_{mpp} \cdot I_{pv} - V_{mpp} \cdot I_S \cdot \exp\left[\frac{V_{mpp} + I_{mpp} \cdot I_S}{A \cdot N_S \cdot V_t}\right] + V_{mpp} \cdot I_S - P_{\max,e}} \tag{23}$$

According to [18], its initial value is given by:

$$R_{p,\min} = \frac{V_{mpp}}{I_{sc} - I_{mpp}} - \frac{V_{oc} - V_{mpp}}{I_{mpp}} \tag{24}$$

The saturation current I_S can be calculated by subsisting the Eq. (11) into Eq. (3), while considering that R_P is very high. This leads to the following equation.

$$I_S = \frac{I_{SC}}{\exp\left(\frac{V_{OC}}{A \cdot N_S \cdot V_t}\right) - 1} \tag{25}$$

To identify R_S, an algorithm is presented in the flow chart shown in Fig. 2.

3.1.2. Estimation method II

The fact that Eq. (1) does not admit an explicit solution is an important limitation. This limitation can be overcome by using the Lambert W function [19].

Eq. (6) can be rearranged to express R_P as a function of R_S as shown in Eq. (26).

$$R_p = \frac{V_{mpp} + I_{mpp} \cdot R_S}{I_{pv} - I_{mpp} - I_S \cdot \left[\exp\left(\frac{V_{mpp} + I_{mpp} \cdot R_S}{A \cdot N_S \cdot V_t}\right) - 1\right]} \tag{26}$$

If we make the following change of variable:

$$x = \frac{V_{mpp} + R_S \cdot I_{mpp}}{A \cdot N_S \cdot V_t} \tag{27}$$

Then the series and parallel resistances can be written as follows:

$$R_S = \frac{x \cdot A \cdot N_S \cdot V_t - V_{mpp}}{I_{mpp}} \tag{28}$$

$$R_P = \frac{x \cdot A \cdot N_S \cdot V_t}{I_{pv} - I_{mpp} - I_S \cdot (\exp(x) - 1)} \tag{29}$$

According to [19], Eq. (7) admits an analytical solution based on the use of the Lambert W function, which is the solution of the equation:

$$f(x) = x \cdot e^x \tag{30}$$

where x's expression is given in Eq. (31). The value obtained by (31) is substituted in (28) and (29) to deduce the values of R_P and R_S.

$$x = \text{Lambert W}\left[\frac{V_{mpp} \cdot (2I_{mpp} - I_{PV} - I_S)\exp\left(\frac{V_{mpp}(V_{mpp} - 2A \cdot V_t)}{A^2 \cdot N_S^2 \cdot V_t^2}\right)}{A \cdot N_S \cdot V_t \cdot I_S}\right] + 2 \cdot \frac{V_{mpp}}{A \cdot N_S \cdot V_t} - \frac{V_{mpp}^2}{A^2 \cdot N_S^2 \cdot V_t^2} \tag{31}$$

The diode reverse saturation current is assumed to vary with temperature according to [19]. Its expression is given by:

$$I_S = I_{pvn} \cdot \exp\left(-\frac{V_{ocn}}{A \cdot N_S \cdot V_{tn}}\right) \tag{32}$$

The photocurrent is calculated by the following equation:

$$I_{pv} \approx I_{scn} \tag{33}$$

Identically to Method I, the ideality factor is calculated by Eq. (21).

To implement these methods using the above equations and the manufacturer's datasheet of the three modules mentioned in Table 1, a set of programs is developed in script files in MATLAB environment.

3.2. The various mathematical modeling equations

PV modules normally function under changing environmental conditions, namely, irradiance and temperature. These conditions affect their output power. Therefore, it is essential for them to be considered in modeling. Most modeling studies considered that R_S, R_P and A are constant and independent of temperature and irradiance's variations. The only parameters that are considered changing are I_S and I_{PV}. To evaluate these two parameters, a combination of five equations is used in the literature for all mathematical models, which are classified as follows:

Model 1 [13–15] assumes that the open circuit voltage and the short circuit current depend on temperature, and are given respectively as follows:

$$V_{oc} = V_{ocn} + K_v \cdot dT \tag{34}$$

$$I_{sc} = I_{scn} + K_i \cdot dT \tag{35}$$

Eqs. (3) and (4) can be written as (36) and (37) respectively:

$$I_S = \frac{I_{scn} + K_i \cdot dT}{\exp\left(\frac{V_{ocn} + K_v \cdot dT}{A \cdot N_S \cdot V_t}\right)} + \frac{R_S \cdot (I_{scn} + K_i \cdot dT) - (V_{ocn} + K_v \cdot dT)}{R_p \cdot \exp\left(\frac{V_{ocn} + K_v \cdot dT}{A \cdot N_S \cdot V_t}\right)} \tag{36}$$

$$I_{pv} = \frac{G}{G_n}\left[I_S\left\{\exp\left(\frac{V_{ocn} + K_v \cdot dT}{A \cdot N_S \cdot V_t}\right) - 1\right\} + \frac{V_{ocn} + K_v \cdot dT}{R_p}\right] \tag{37}$$

Model 2 [13–15]: the authors considered (11), while assuming that the resistance R_P is very high.

Table 1
Manufacturer's data of the three modules used at STC.

Parameters	Multicrystalline Kyocera KC200GT	Monocrystalline Shell SQ80	Thin-film Shell ST40
N_S	54	36	42
I_{SC} (A)	8.21	4.85	2.68
V_{OC} (V)	32.9	21.8	23.3
V_{mpp} (V)	26.3	17.5	16.6
I_{mpp} (A)	7.61	4.58	2.41
K_I (mA/°C)	3.18	1.4	0.35
K_V (mV/°C)	−123	−81	−100

Rearranging Eq. (3) we obtain the same expression of I_S as in Eq. (25).

Using Eqs. (34) and (35) that characterize the dependence of V_{OC} and I_{SC} on temperature, Eq. (25) can be rewritten in the following form:

$$I_S = \frac{I_{scn} + K_i \cdot dT}{\exp\left(\frac{V_{ocn} + K_v \cdot dT}{A \cdot N_S \cdot V_t}\right) - 1} \tag{38}$$

while the photocurrent can be written as:

$$I_{pv} = \frac{G}{G_n}(I_{pvn} + K_i \cdot dT) \tag{39}$$

Model 3 [13–15,20,21]: This model is based on the fact that the value of R_P is very high at STC. Consequently, Eq. (3) becomes:

$$I_{Sn} = \frac{I_{pvn}}{\exp\left(\frac{V_{OC}}{A \cdot N_S \cdot V_t}\right) - 1} \tag{40}$$

Hence the following expression of V_{OC}:

$$V_{OC} = \frac{A \cdot N_S \cdot k \cdot T}{q} \ln\left(\frac{I_{pvn}}{I_{sn}} + 1\right) \tag{41}$$

Using the following expression of V_{OC}:

$$V_{OC}(G,T) - V_{OC}(G,T_n) = -|K_V|dT \tag{42}$$

Eq. (40) is injected into Eq. (41) to express the difference between $V_{OC}(G, T)$ and $V_{OC}(G, T_n)$ shown in the following equation:

$$\frac{A \cdot N_S \cdot k}{q}\left[T \ln\left(\frac{\frac{G}{G_n}(I_{scn} + K_i \cdot dT)}{I_S} + 1\right) - T_n \ln\left(\frac{\frac{G}{G_n} \cdot I_{scn}}{I_{Sn}} + 1\right)\right] = -|K_V|dT \tag{43}$$

Rearranging (43), I_S becomes:

$$I_S = \frac{\frac{G}{G_n} \cdot (I_{scn} + K_i \cdot dT) \cdot \exp\left(\frac{q \cdot |K_V| \cdot dT}{A \cdot N_S \cdot k \cdot T}\right)}{\left(\frac{\frac{G}{G_n} \cdot I_{scn}}{I_{Sn}} + 1\right)^{\frac{T_n}{T}} - \exp\left(\frac{q \cdot |K_V| \cdot dT}{A \cdot N_S \cdot k \cdot T}\right)} \tag{44}$$

And the photocurrent is expressed as in Eq. (39), or as follows:

$$I_{pv} = \frac{G}{G_n}(I_{SC} + K_i \cdot dT) \tag{45}$$

Model 4 [13–15] is based on the fact that the reverse saturation current of the diode is dependent on the temperature as well as on the band gap energy.

$$I_S = I_{Sn} \cdot \left(\frac{T}{T_n}\right)^3 \cdot \exp\left(\frac{q \cdot E_g}{A \cdot k}\left(\frac{1}{T_n} - \frac{1}{T}\right)\right) \tag{46}$$

With: $I_{Sn} = \frac{I_{scn} \cdot \left(1 + \frac{R_S}{R_P}\right)}{\exp\left(\frac{V_{ocn}}{A \cdot N_S \cdot V_t}\right) - 1}$

The photocurrent's expression stays the same as Eq. (39).

Table 2
The estimated parameters of Kyocera KC200GT using Methods I and II at STC.

Parameters	The estimated values	
	Method I	Method II
A	1.075812	1.075816
R_S (Ω)	0.308000	0.284057
R_P (Ω)	193.049394	157.853220
I_S (A)	2.152360×10^{-9}	2.195410×10^{-9}
I_{PV} (A)	8.223300	8.210000

Table 3
The estimated parameters of Shell SQ80 using Methods I and II at STC.

Parameters	The estimated values	
	Method I	Method II
A	1.065135	1.065136
R_S (Ω)	0.308000	0.306027
R_P (Ω)	1368.228524	1339.348911
I_S (A)	1.186410×10^{-9}	1.190430×10^{-9}
I_{PV} (A)	4.851197	4.850000

Table 4
The estimated parameters of Shell ST40 using Methods I and II at STC.

Parameters	The estimated values	
	Method I	Method II
A	1.134544	1.134550
R_S (Ω)	1.494000	1.372319
R_P (Ω)	257.165987	194.663910
I_S (A)	1.4137×10^{-9}	1.45487×10^{-9}
I_{PV} (A)	2.695670	2.680000

Model 5 [21] assumes that V_{OC} depends not only on temperature but also on irradiance. A new equation relating V_{OC} with V_{ocn} is issued:

$$V_{oc} = V_{ocn} + K_V \cdot dT + A \cdot N_S \cdot V_t \cdot \ln\left(\frac{G}{G_n}\right) \tag{47}$$

Evaluating Eq. (1) provided at (V_{OC}, 0) to express I_{pvn}, then at (0, I_{SC}) to express I_{SC} and substituting I_{pvn} in I_{SC}'s equation yields:

$$I_S = \frac{\left(1 + \frac{R_S}{R_p}\right)I_{sc} - \frac{V_{oc}}{R_p}}{\exp\left(\frac{V_{oc}}{A \cdot N_S \cdot V_t}\right) - \exp\left(\frac{R_S \cdot I_{sc}}{A \cdot N_S \cdot V_t}\right)} \tag{48}$$

By substituting (35) and (47) into (48), we obtain Eq. (49).

$$I_S = \frac{\left(1 + \frac{R_S}{R_p}\right)(I_{scn} + K_i \cdot dT) - \frac{V_{ocn} + K_V \cdot dT + A \cdot N_S \cdot V_t \cdot \ln\left(\frac{G}{G_n}\right)}{R_p}}{\exp\left(\frac{V_{ocn} + K_V \cdot dT + A \cdot N_S \cdot V_t \cdot \ln\left(\frac{G}{G_n}\right)}{A \cdot N_S \cdot V_t}\right) - \exp\left(\frac{(I_{scn} + K_i \cdot dT)R_S}{A \cdot N_S \cdot V_t}\right)} \tag{49}$$

Again, the photocurrent is calculated by Eq. (39).

The five models described above have been verified, validated and tested on three types of PV modules (multicrystalline, monocrystalline, and thin-film), while changing the temperature and irradiance, to determine the most accurate among them.

4. Simulation results and discussions

4.1. Validation of different models

The equations of the previous section were implemented in MATLAB/Simulink environment to simulate, evaluate and test the five models by means of the two estimation methods mentioned above for three different modules, namely, KC200GT, SQ80, and ST40. The datasheet parameters specified under STC are already given in Table 1. Tables 2–4 show the parameters estimated for these modules using methods I and II. These parameters are used to evaluate and test the different estimation methods and models discussed in the previous section. The values of R_S, R_P, A, I_S and I_{PV} are estimated using both methods. Certainly, the similarity of the results between method I and II is noteworthy and the differences have no appreciable influence on the simulated I–V characteristics at STC. However, when analyzing Fig. 11, it is clear that the small differences in the parameter values at STC lead to different

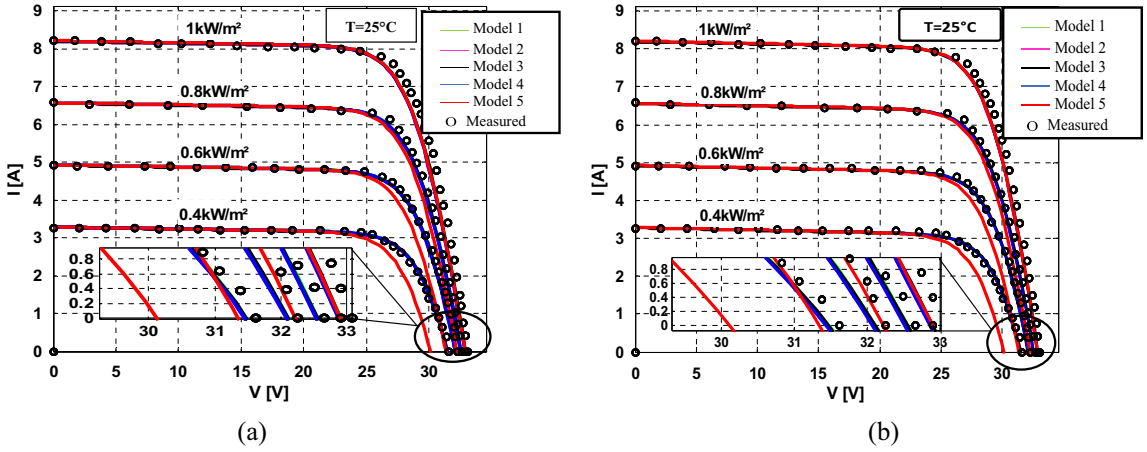

Fig. 3. *I–V* characteristic for Kyocera KC200GT module under varying irradiance for models 1, 2, 3, 4, and 5 and measured values, using parameter estimation methods; (a) method I, (b) method II.

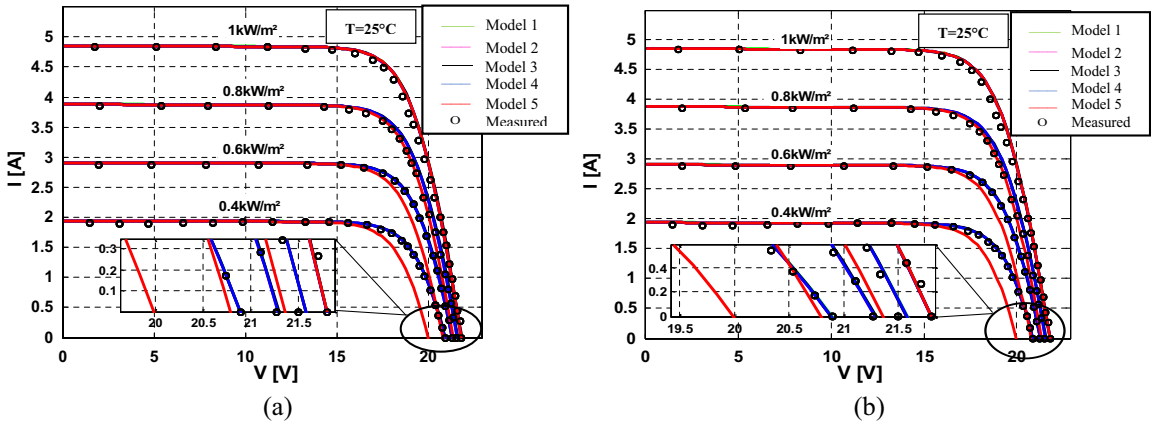

Fig. 4. *I–V* characteristic for Shell SQ80 module under varying irradiance for models 1, 2, 3, 4, and 5 and measured values, using parameter estimation methods; (a) Method I, (b) Method II.

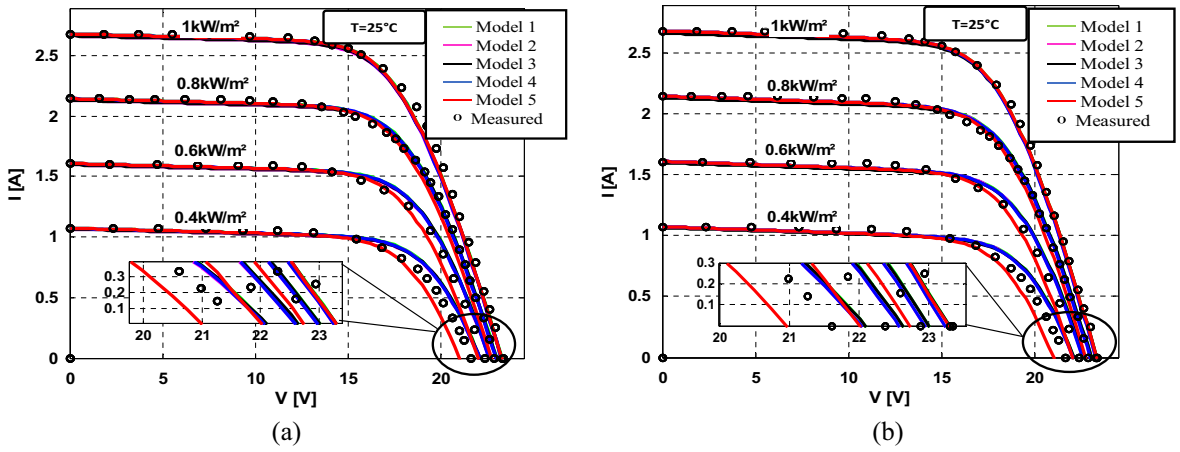

Fig. 5. *I–V* characteristic for Shell ST40 module under varying irradiance for models 1, 2, 3, 4, and 5 and measured values, using parameter estimation methods; (a) Method I, (b) Method II.

behavior of the translation models, at least for the thin-film module. The only cause of the better performance of method II with respect to method I for the thin-film module is that it has been able to adjust better the five unknown parameters at STC.

4.1.1. Irradiance effect

Figs. 3–5 show the reconstructed five models' *I–V* characteristics using the parameters estimated with methods I and II described above. These *I–V* characteristics are compared with

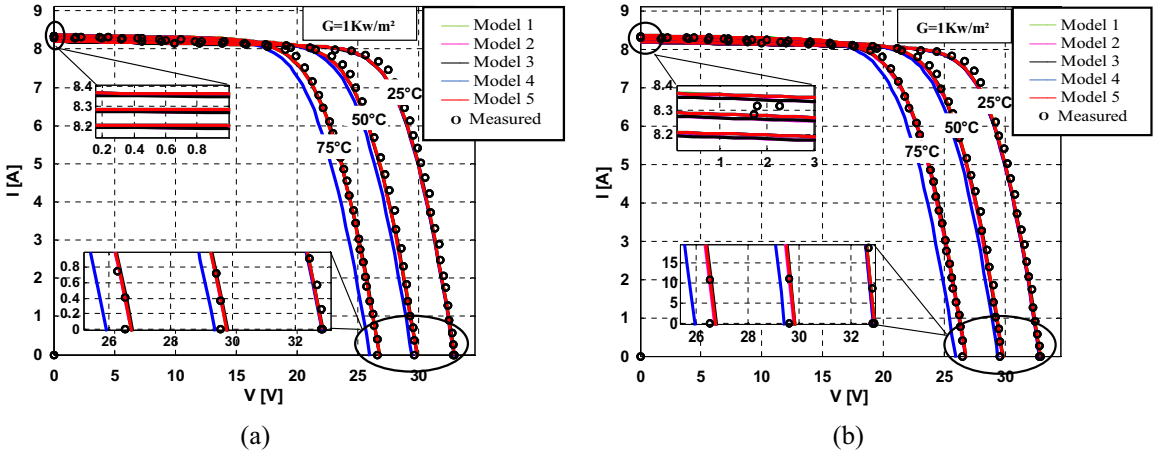

Fig. 6. *I–V* characteristic for Kyocera KC200GT module under varying temperature for models 1, 2, 3, 4, and 5 and measured values, using parameter estimation methods; (a) Method I, (b) Method II.

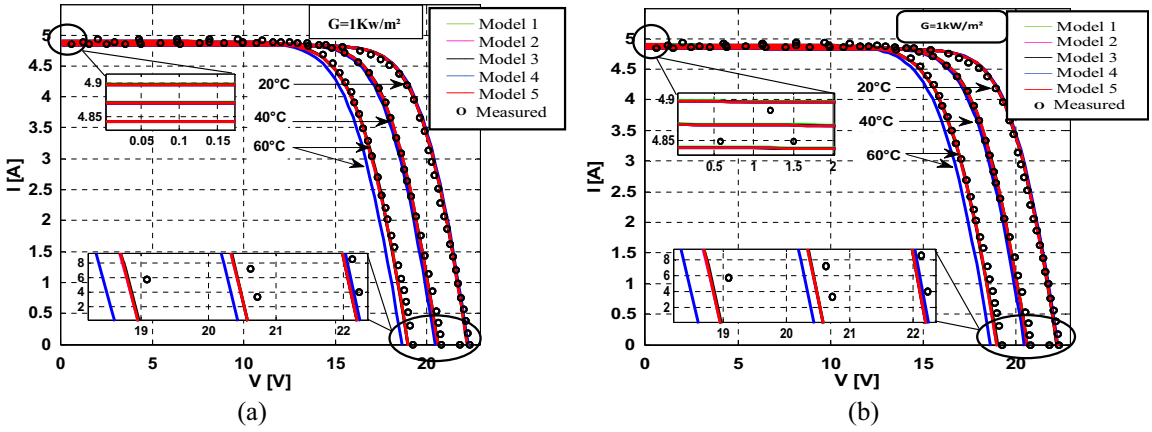

Fig. 7. *I–V* characteristic for Shell SQ80 module under varying temperature for models 1, 2, 3, 4, and 5 and measured values, using parameter estimation methods; (a) Method I, (b) Method II.

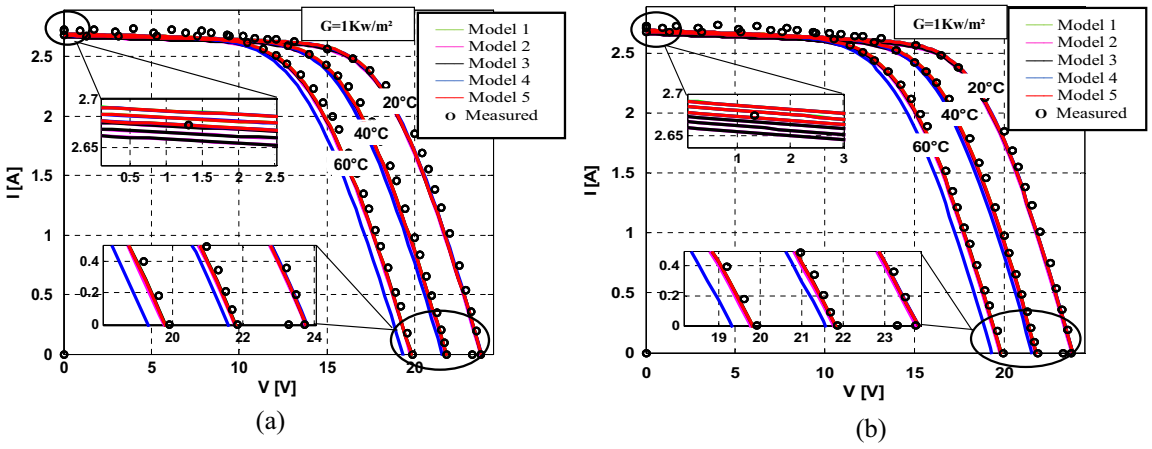

Fig. 8. *I–V* characteristic for Shell ST40 module under varying temperature for models 1, 2, 3, 4, and 5 and measured values, using parameter estimation methods; (a) Method I, (b) Method II.

measured data extracted from each PV module's datasheet, for different irradiance levels ranging from 0.4 kW/m^2 up to 1 kW/m^2 at a fixed temperature of 25 °C. It is observed that the module's output currents depend heavily on the solar irradiance, because they vary linearly with it. When the irradiance decreases, the intensity of the short circuit current I_{SC} also decreases, while the open circuit voltages V_{OC} undergo only a small variation. It is noted that the *I–V* characteristics of the five models show good agreement with the measured data for both methods, with the exception of model 5 around V_{OC}, for which the characteristic tends to deviate relatively

away from the characteristics of models 1, 2, 3 and 4 for low irradiance. This deviation can be explained using the saturation current Eq. (49)in model 5 which demonstrates the dependence of V_{OC} on irradiance. In addition to this factor, Siddique et al. [22] explained that there is a logarithmic dependence between the V_{OC} and the irradiance as shown in Eq. (47), which is clearly illustrated in Figs. 3–5 where the dependence of V_{OC} on irradiance is significant at low irradiance. For both recommended methods, the equation used for calculating I_{PV} is the same for all models except model 1, which explains the similarity of the short circuit current response for all models. It can also be noted that even at low irradiance the accuracy of all models is maintained except that of model 5. Therefore, the behavior of all PV modules is independent of the method used to estimate their parameters.

4.1.2. Temperature effect

The temperature is a very influential parameter on the behavior of PV modules since they are exposed to the sun. Figs. 6–8 show the reconstructed five models' *I–V* characteristics using the parameters estimated with methods I and II described above. These *I–V* characteristics are compared with measured data extracted from each of the PV module's datasheet, for different temperature levels and at a fixed irradiance of 1 kW/m^2. According to the *I–V* characteristics, except for model 4, it is noted that the simulation results of the five models implemented indicate a high agreement between the measured data and the *I–V* reconstructed characteristics, using method I and II, under varying temperature. It can be seen that the temperature effect on the short circuit current is the same for all models. On the one hand, this basically shows that there is minimal dependence between I_{SC} and temperature changes. On the other hand, V_{OC} undergoes a remarkable decrease. It is observed that at temperatures around STC, the models have similar behavior for both methods. However, as the temperature increases, one of the model's characteristics tends to deviate from the others, i.e. the one characterizing model 4. This deviation is due to the increase in temperature which reduces the band gap energy, consequently increasing the saturation current I_S as shown in Eq. (46). The same explanation is given by [44] who mentioned that I_S adjusts the predicted voltage at all points on the *I–V* characteristics.

4.2. Validation of modeling methods

The accuracies of the estimation methods and various models listed above were compared using the RMSE given by Eq. (50) [22], where y_i is the calculated value (current or voltage), x_i is the measured value (current or voltage) provided by the manufacturer, and n is the number of points in [0, V_{ocn}].

The RMSE is a statistical indicator that refers to the standard deviation between the calculated and measured data, and can be used to measure both systematic and unsystematic errors. It is more appropriate to use the RMSE than the other indicators when the model errors follow a normal distribution [22].

$$\mathrm{RMSE} = \frac{1}{n}\left[\sum_{i=1}^{n}(y_i - x_i)^2\right]^{1/2} \div \left[\frac{1}{n}\sum_{i=1}^{n}x_i\right] \tag{50}$$

Figs. 9–11 present a comparative analysis of the five models' current and voltage relative errors, using both methods of estimation for the three modules KC200GT, SQ80 and ST40 under variable irradiance and temperature.

For both methods, when the irradiance decreases, the current errors also decrease for all the models except for model 3, where a rapid increase is noticed (0.25–0.67) for KC200GT and (0.58–1.32) for SQ80 as shown in Figs. 9 and 10. However, when the temperature rises, on the one hand, the current errors rise slightly for all models except for model 3, which experiences a significant increase (0.23–0.56) for KC200GT and (0.39–0.71) for SQ80 as shown in Figs. 9 and 10. On the other hand, the variation of voltage errors under varying temperature is very small for both KC200GT and SQ80 modules. For the ST40 module, current errors increase as a result of the irradiance drop and the temperature rise, especially for models 2 and 4 for which the variation is between 0.21 up to 0.38 while using method I. For the same models, voltage

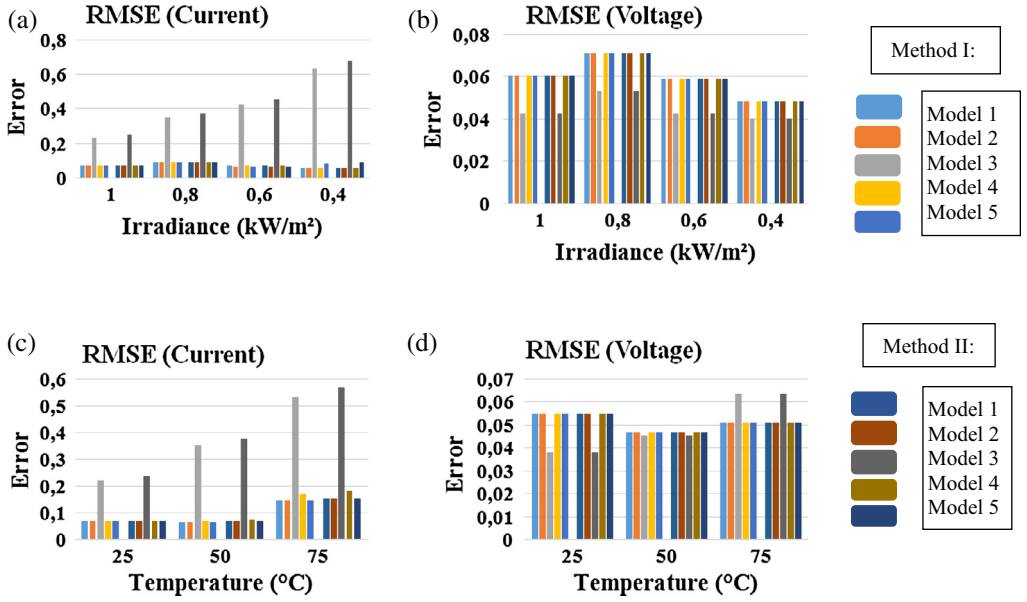

Fig. 9. (a–d) Show the relative error analysis of current and voltage for Kyocera KC200GT using both methods and different models at different levels of irradiance and temperature.

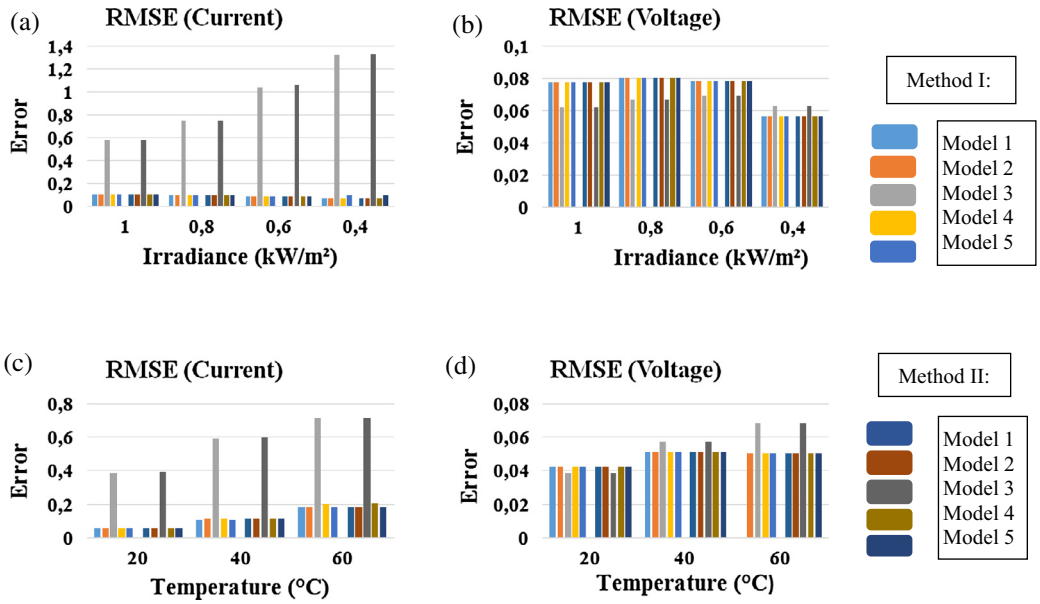

Fig. 10. (a–d) Show the relative error analysis of current and voltage for Shell SQ80 using both methods at different levels of irradiance and temperature.

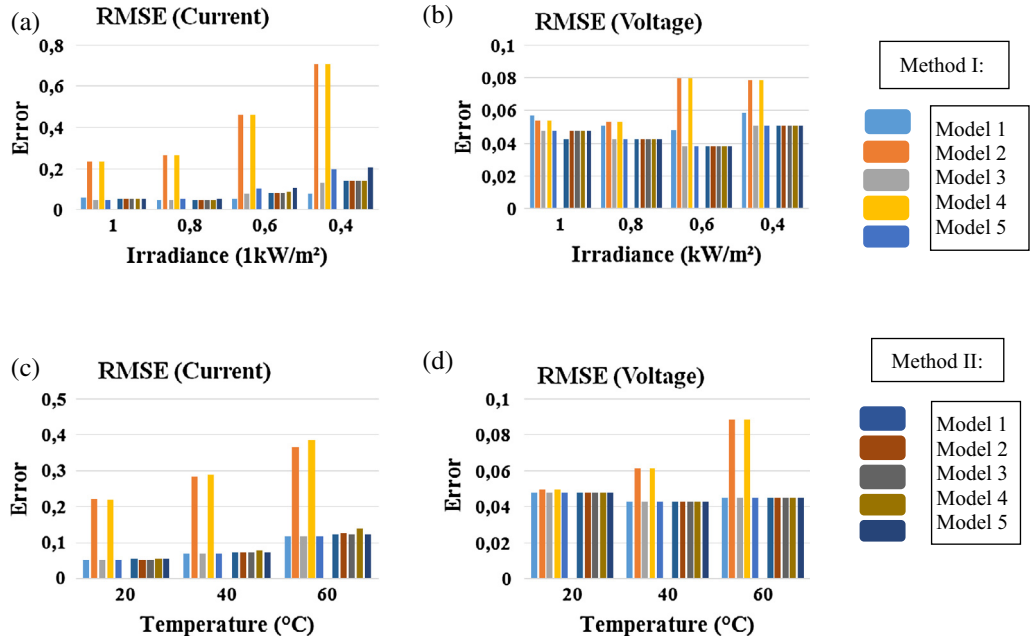

Fig. 11. (a–d) Show the relative error analysis of current and voltage for Shell ST40 using both methods at different levels of irradiance and temperature.

errors are not greatly affected as they are between 0.049 and 0.088. On the other hand, method II presents a good compromise for all models. It offers a good parameter estimation with a small error at low temperature and high irradiance as shown in Fig. 11.

These errors may be attributed to the uncertainty in the extraction of the experimental points. Another reason is the fact that only two parameters were considered variables with environmental changes instead of five.

The results reveal that the behavior of the two methods is almost the same for the monocrystalline and multicrystalline modules, while method II performs appreciably better for the thin-film module. Therefore, the small difference in the estimated parameters at STC does not affect the performance of the five models for the monocrystalline and multicrystalline modules, but it does affect the performance of the models for the thin-film module (especially the performance of models 1, 2 and 4). Another finding is that for the monocrystalline and multicrystalline modules, models 1, 2, 4 and 5 have practically the same performance, while model 3 shows the worst results in the current errors and the best results in the voltage errors (except at high temperatures, where the voltage errors increase).

5. Conclusion

In this work, different parameter estimation methods as well as five models existing in the literature are described and have been verified by simulation and measured data, which were extracted

from datasheet *I–V* characteristics. The models that best approximate the *I–V* characteristics given in the PV modules' datasheets of both SQ80 and KC200GT modules are model 1 and model 2. As for the ST40 module, it's shown that the most accurate method of parameter estimation is method II as it presents fewer errors in comparison to method I, combined with models 1, 2 and 3. The differences between the two estimation methods have no appreciable influence on the simulated *I–V* characteristics under varying environmental conditions. In particular, excellent accuracy exhibited at high irradiance and low temperature conditions for all models. It is envisaged that this study can be a valuable design tool for PV system designers.

References

[1] Ministry of Energy, Mines, Water and Environment. Law no. 58-15 amending and supplementing law no. 13-09 relating to renewable energy. <http://www.mem.gov.ma/SitePages/GrandChantiersEn/DEREELaw58-15.aspx>.

[2] National Office of Electricity and Water Supply (ONEE). Project Noor-Tafilalt, Noor-Atlas, and Noor-Argana. <http://www.one.org.ma>.

[3] Kousksou T, Allouhi A, Belattar M, Jamil A, El Rhafiki T, Arid A, et al. Renewable energy potential and national policy directions for sustainable development in Morocco. Renew Sustain Energy Rev 2015;47():46–57.

[4] Allouhi A, Jamil A, Kousksou T, El Rhafiki T, Mourad Y, Zeraouli Y. Solar domestic heating water systems in Morocco: an energy analysis. Energy Convers Manage 2015;92:105–13.

[5] Zeng K, Gauthier D, Lu J, Flamant G. Parametric study and process optimization for solar pyrolysis of beech wood. Energy Convers Manage 2015;106:987–98.

[6] Najibi F, Niknam T. Stochastic scheduling of renewable micro-grids considering photovoltaic source uncertainties. Energy Convers Manage 2015;98:484–99.

[7] Cao S, Sirén K. Matching indices taking the dynamic hybrid electrical and thermal grids information into account for the decision-making of nZEB on-site renewable energy systems. Energy Convers Manage 2015;101:423–41.

[8] Chiaroni D, Chiesa V, Colasanti L, Cucchiella F, D'Adamo I, Frattini F. Evaluating solar energy profitability: a focus on the role of self-consumption. Energy Convers Manage 2014;88:317–31.

[9] De Arce R, Mahía R, Medina E, Escribano G. A simulation of the economic impact of renewable energy development in Morocco. Energy Policy 2012;31(46):335–45.

[10] Hanger S, Komendantova N, Schinke B, Zejli D, Ihlal A, Patt A. Community acceptance of large-scale solar energy installations in developing countries: evidence from Morocco. Energy Res Soc Sci 2016;14:80–9.

[11] Cucchiella F, D'Adamo I. Issue on supply chain of renewable energy. Energy Convers Manage 2013;76:774–80.

[12] Tali M, Obbadi A, Elfajri A, Errami Y. Passive filter for harmonics mitigation in standalone PV system for non linear load. In: Renewable and sustainable energy conference (IRSEC), 2014 international. IEEE; 2014. p. 499–504.

[13] Shongwe S, Hanif M. Comparative analysis of different single-diode PV modeling methods. Photovoltaics, IEEE J 2015;5(3):938–46.

[14] Chin VJ, Salam Z, Ishaque K. Cell modelling and model parameters estimation techniques for photovoltaic simulator application: a review. Appl Energy 2015;154:500–19.

[15] Humada AM, Hojabri M, Mekhilef S, Hamada HM. Solar cell parameters extraction based on single and double-diode models: a review. Renew Sustain Energy Rev 2016;56:494–509.

[16] Cristaldi L, Faifer M, Rossi M, Ponci F. A simple photovoltaic module model: characterization procedure and evaluation of the role of environmental measurements. Instrum Meas, IEEE Trans 2012;61(10):2632–41.

[17] Bai J, Liu S, Hao Y, Zhang Z, Jiang M, Zhang Y. Development of a new compound method to extract the five parameters of PV modules. Energy Convers Manage 2014;31(79):294–303.

[18] Villalva MG, Gazoli JR. Comprehensive approach to modeling and simulation of photovoltaic arrays. Power Electron, IEEE Trans 2009;24(5):1198–208.

[19] Femia N, Petrone G, Spagnuolo G, Vitelli M. Power electronics and control techniques for maximum energy harvesting in photovoltaic systems. CRC Press; 2012.

[20] Ismail MS, Moghavvemi M, Mahlia TMI. Characterization of PV panel and global optimization of its model parameters using genetic algorithm. Energy Convers Manage 2013;73:10–25.

[21] Mahmoud YA, Weidong X, Zeineldin HH. A parameterization approach for enhancing PV model accuracy. Ind Electron, IEEE Trans 2013;60(12):5708–16.

[22] Siddique HAB, Ping X, De Doncker RW. Parameter extraction algorithm for one-diode model of PV panels based on datasheet values. In: Clean electrical power (ICCEP), 2013 international conference on IEEE. p. 7–13.

[23] KC200GT High Efficiency Multicrystal Photovoltaic Module Datasheet Kyocera. 2000. <http://www.kyocera.com.sg/products/solar/pdf/kc200gt.pdf>.

[24] Shell Solar Product Information Sheet. <http://www.solarcellsales.com/techinfo/technical_docs.cfm>.

[25] Tamrakar R, Gupta A. A review: extraction of solar cell modelling parameters. Int J Innovative Res Electr, Electron, Instrum Control Eng 2015;3(1).

[26] Ayodele TR, Ogunjuyigbe AS, Ekoh EE. Evaluation of numerical algorithms used in extracting the parameters of a single-diode photovoltaic model. Sustain Energy Technol Assess 2016;13:51–9.

[27] Batzelis EI, Routsolias IA, Papathanassiou SA. An explicit PV string model based on the Lambert function and simplified MPP expressions for operation under partial shading. Sustain Energy, IEEE Trans 2014;5(1):301–12.

[28] Cubas J, Pindado S, Manuel Cde. Explicit expressions for solar panel equivalent circuit parameters based on analytical formulation and the Lambert W-Function. Energies 2014;7:4098–115.

[29] Khatib T, Sopian K, Kazem HA. Actual performance and characteristic of a grid connected photovoltaic power system in the tropics: a short term evaluation. Energy Convers Manage 2013;31(71):115–9.

[30] Moballegh S, Jiang J. Modeling, prediction, and experimental validations of power peaks of PV arrays under partial shading conditions. Sustain Energy, IEEE Trans 2014;5(1):293–300.

[31] Rahman SA, Varma RK, Vanderheide T. Generalised model of a photovoltaic panel. Renew Power Generation, IET 2014;8(3):217–29.

[32] Navabi R, Abedi S, Hosseinian SH, Pal R. On the fast convergence modeling and accurate calculation of PV output energy for operation and planning studies. Energy Convers Manage 2015;89:497–506.

[33] Mares O, Paulescu M, Badescu V. A simple but accurate procedure for solving the five-parameter model. Energy Convers Manage 2015;15(105):139–48.

[34] Soon JJ, Low KS. Photovoltaic model identification using particle swarm optimization with inverse barrier constraint. Power Electron, IEEE Trans 2012;27(9):3975–83.

[35] Askarzadeh A, dos Santos Coelho L. Determination of photovoltaic modules parameters at different operating conditions using a novel bird mating optimizer approach. Energy Convers Manage 2015;89:608–14.

[36] Guo L, Meng Z, Sun Y, Wang L. Parameter identification and sensitivity analysis of solar cell models with cat swarm optimization algorithm. Energy Convers Manage 2016;15(108):520–8.

[37] Askarzadeh A, Rezazadeh A. Artificial bee swarm optimization algorithm for parameters identification of solar cell models. Appl Energy 2013;102:943–9.

[38] Awadallah MA. Variations of the bacterial foraging algorithm for the extraction of PV module parameters from nameplate data. Energy Convers Manage 2016;1(113):312–20.

[39] Alam DF, Yousri DA, Eteiba MB. Flower pollination algorithm based solar PV parameter estimation. Energy Convers Manage 2015;101:410–22.

[40] Muhsen DH, Ghazali AB, Khatib T, Abed IA. Extraction of photovoltaic module model's parameters using an improved hybrid differential evolution/electromagnetism-like algorithm. Sol Energy 2015;30(119):286–97.

[41] Barukčić M, Ćorluka V, Miklošević K. The irradiance and temperature dependent mathematical model for estimation of photovoltaic panel performances. Energy Convers Manage 2015;1(101):229–38.

[42] Bonanno F, Capizzi G, Graditi G, Napoli C, Tina GM. A radial basis function neural network based approach for the electrical characteristics estimation of a photovoltaic module. Appl Energy 2012;30(97):956–61.

[43] Fathabadi H. Novel neural-analytical method for determining silicon/plastic solar cells and modules characteristics. Energy Convers Manage 2013;31(76):253–9.

[44] Boyd MT, Klein SA, Reindl DT, Dougherty BP. Evaluation and validation of equivalent circuit photovoltaic solar cell performance models. J Sol Energy Eng 2011;133(2):021005.